# Supporting Information

## Manipulation of $Cs_{0.1}FA_{0.9}PbI_3$ crystallization behavior towards efficient carbon-based printable mesoscopic perovskite solar cells

Jinjiang Wang,[ab] Dongjie Wang,*[a] Yang Zhang,[a] Yiwen Chen,[a] Tianhuan Huang,[a] Wending Zhu,[a] Zheling Zhang,[a] Yu Huang,[a] Jian Xiong,[a] Dinghan Xiang,[a] Jian Zhang*[a]

[a] Engineering Research Center of Electronic Information Materials and Devices of Ministry of Education, Guangxi Key Laboratory of Information Materials, School of Materials Science and Engineering, School of Mechanical and Electrical Engineering, Guilin University of Electronic Technology, Guilin 541004, China

[b] School of Physics and Electronics Engineering, Hengyang Normal University, Hengyang 421002, China

* Corresponding author: Prof. J. Zhang, E-mail: jianzhang@guet.edu.cn; Dr. D. Wang, E-mail: djwang@guet.edu.cn

## Experimental section

### Materials and Reagents

Formamidinium Iodide (FAI, ≥ 99.5%), cesium iodide (CsI ≥ 99.9%) and lead (II) iodide ($PbI_2$, > 99.99%) were purchased from Xi'an Polymer Light Technology Corp. Propylamine hydrochloride (PACl, 98%) was purchased from Innochem. Titanium diisopropoxide bis(acetylacetonate) (75 wt % in isopropanol) and anhydrous solvents such as N,N-Dimethylformamide (DMF, 99.8%) and dimethylsulfoxide (DMSO, ≥99.9%) were purchased from Sigma-Aldrich. $TiO_2$, $ZrO_2$, carbon pastes, and FTO glass sheets were provided by Wonder Solar Corp. All the materials and reagents were used without further purification.

### Precursor Solution Preparation

The $Cs_{0.1}FA_{0.9}PbI_3$ perovskite precursor solution was prepared as follows: 0.186 g of FAI, 0.031 g of CsI, 0.553 g of $PbI_2$, and appropriate quantities of PACl were dissolved in 1 mL of DMF/DMSO (4:1, v/v) mixed solutions and then stirred at 45 °C for 2 h. The compact-$TiO_2$ (c-$TiO_2$) precursor was prepared by mixing 79 g of isopropanol and 9.7 g of titanium di-isopropoxide bis(acetylacetonate), which were stored in the refrigerator before use.

### Device Fabrication

Fluorine-incorporated tin oxide (FTO) conducting glass was etched with a laser to separate the electrodes and then cleaned by sequential ultrasonication with detergent, deionized water and ethanol in turn. A *ca.* 30 nm-thick c-$TiO_2$ layer was deposited on the as-prepared FTO by spray pyrolysis of the c-$TiO_2$ precursor at 450 °C for 20 min. Subsequently, triple-mesoporous layers, including a *ca.* 500 nm-thick mesoporous-$TiO_2$ (m-$TiO_2$) layer, a *ca.* 2 μm-thick mesoporous-$ZrO_2$ (m-$ZrO_2$) spacer layer, and a *ca.* 10 μm-thick carbon layer, were deposited on the cooling c-$TiO_2$ layer by screen-printed technique layer by layer in air environment (40 ± 10% RH, 30 ± 5℃), which was following by annealing at 500, 400 and 400°C for 40 min, respectively. After cooling down to room temperature, 4.0~4.5 μL of perovskite precursor solution was dropped on the top of the porous carbon layer, and then the device was covered with a self-made glass lid and annealed at 75℃ for 9 h. Both drop coating and annealing

processes were carried out in the air with a relative humidity of 30 ± 10% RH and a temperature of 30 ± 5℃.

**Characterization**

Absorption spectra were recorded using an ultraviolet-visible spectrophotometer (PerkinElmer, Lambda 365, USA). The crystal characteristics of the perovskite films deposited on FTO/m-$TiO_2$ were examined using a X-ray diffractometer (Bruker, D8 Advance, Germany). Morphologies of the perovskite films and devices were observed using a field-emission scanning electron microscope (FEI, Quanta FEG 450, USA). FTIR spectra were obtained using an FTIR spectrometer (Thermo Scientific, Nicolet IS10, USA). The topography images and surface potential were measured by KPFM using an atomic force microscope in the tapping mode (Bruker, MultiMode 8, Germany). The photoluminescence (PL) of the perovskite films deposited on FTO/m-$ZrO_2$ was characterized on a fluorescence spectrophotometer (Edinburgh, FS 5, U.K). XPS spectra were measured with a multifunctional photoelectron spectrometer (Thermo Scientific, Escalab 250Xi, USA). GIWAXS measurement was carried out with a Xeuss 2.0 SAXS/WAXS laboratory beamline using a Cu X-ray source (8.05 keV, 1.54 Å) and a Pilatus 3R 300K detector. The current density-voltage (*J-V*) curves were obtained using a Keithley 2400 digital source meter and were measured in both reverse and forward scan directions with a scan rate of 0.01 V/s. A solar simulator (SAN-EI, XES-40S3, Japan) offered a simulated AM 1.5G illumination of 100 mW $cm^2$. The active area of the devices was set 0.1 $cm^2$ with an opaque black mask with a circular aperture. The IPCE spectra were recorded using a QE-R solar cell quantum efficiency measurement system (Enlitech, QE-R, China).

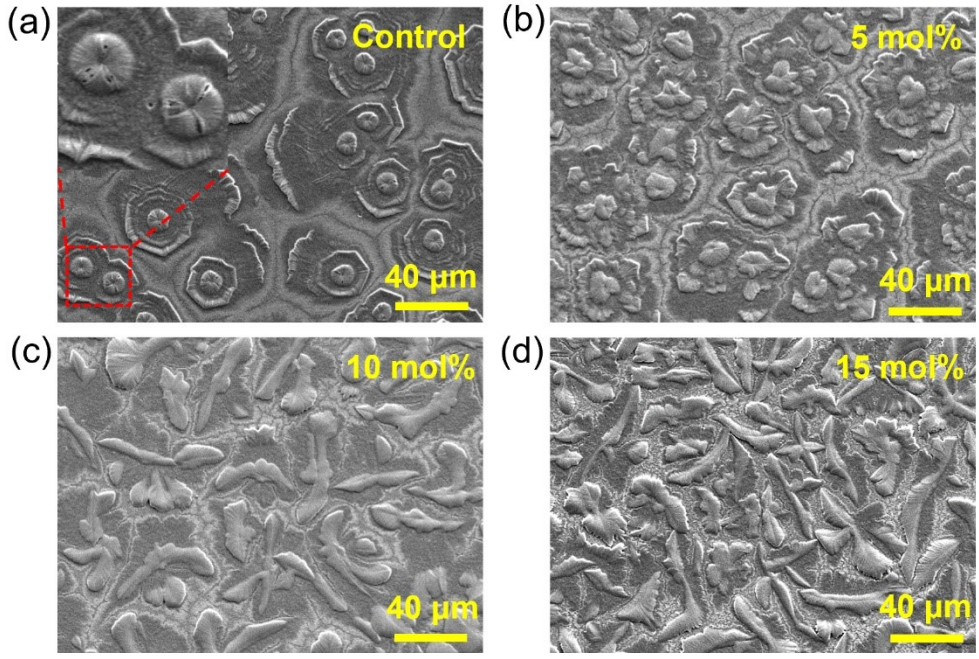


**Fig. S1** Top-view SEM images of the $Cs_{0.1}FA_{0.9}PbI_3$ films spin on the m-$TiO_2$ without and with different concentrations of PACl.

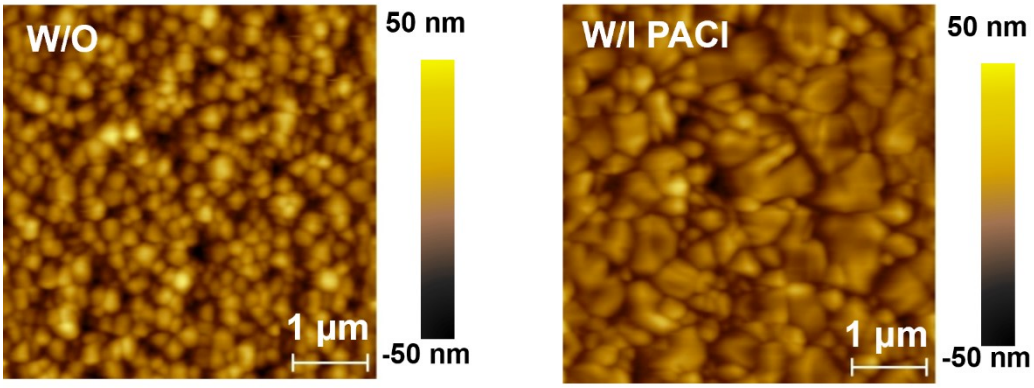


**Fig. S2** AFM images of perovskite films with and without PACl. The scan size of the AFM images was 5 μm × 5 μm.

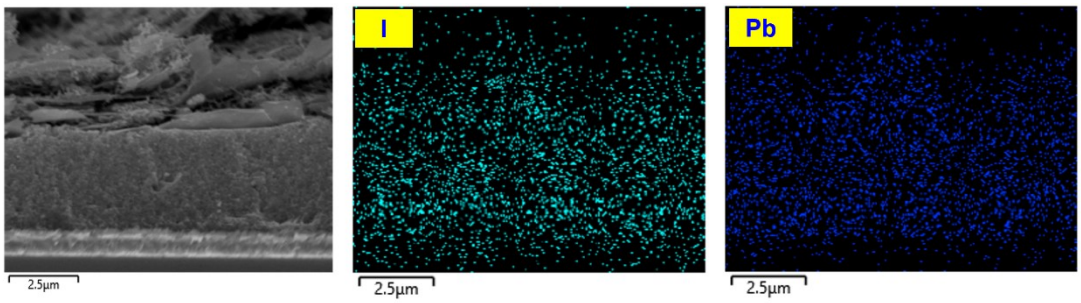


**Fig. S3** Cross-sectional SEM images of the device with PACl and the corresponding element distributions detected by EDS.

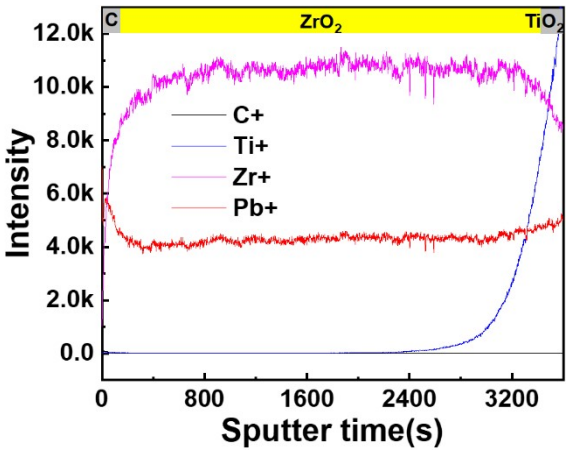


**Fig. S4** TOF-SIMS depth profiles of the $Cs_{0.1}FA_{0.9}PbI_3$ device with PACl.

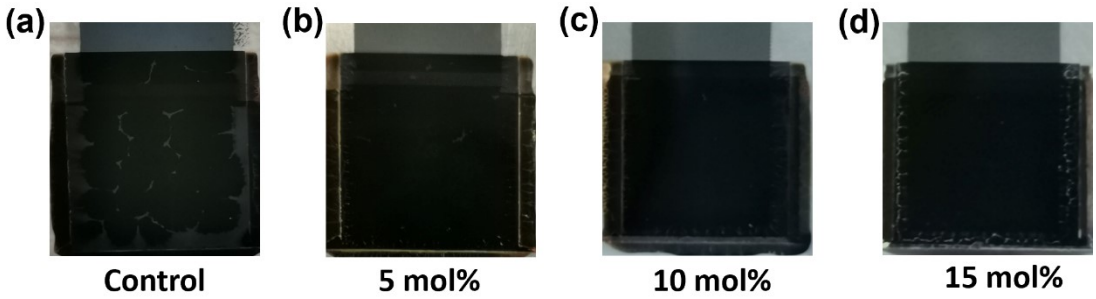


**Fig. S5** Pore filling and crystallization in triple-mesoscopic film of (a) Control, and added (b) 5 mol%, (c) 10 mol%, (d) 15 mol% PACl MPSCs. The photos were taken from the glass side.

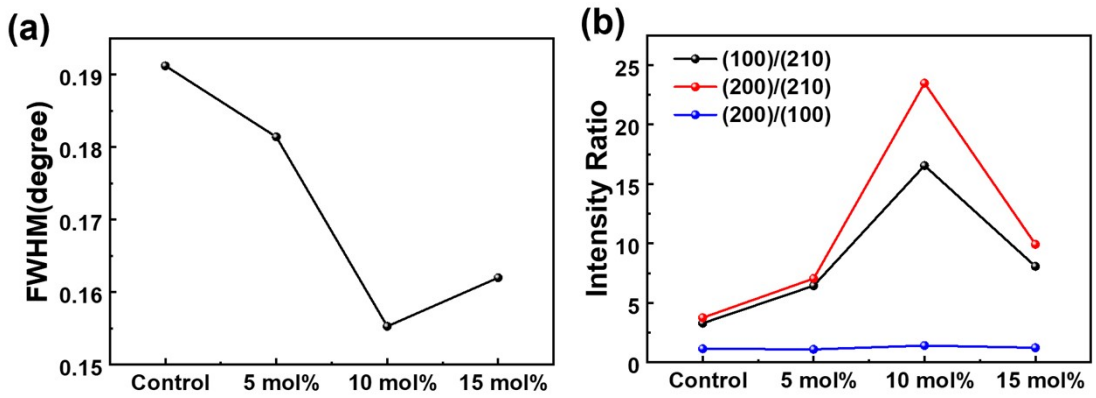


**Fig. S6** (a) FWHM and (b) peak intensity ratio of (100)/(200), (200)/(210), and (200)/(210) with and without PACl.

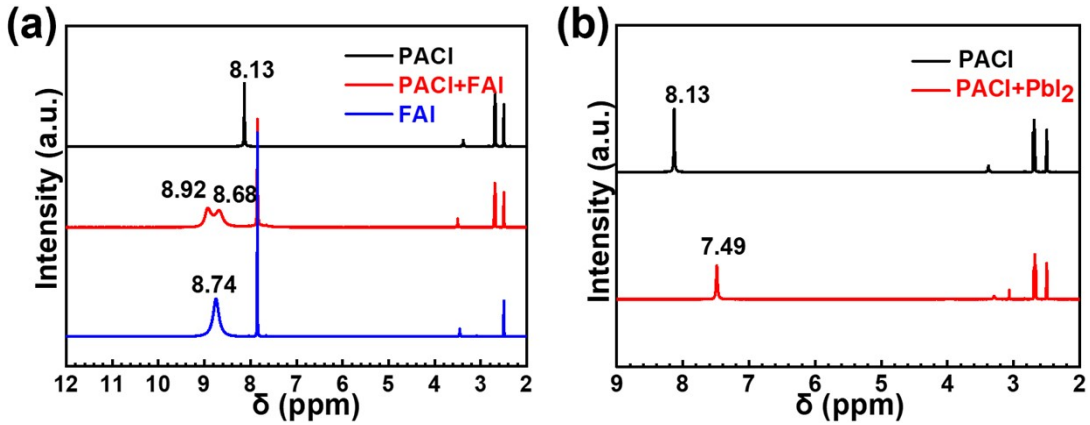


**Fig. S7** $^{1}$H NMR spectrum of (a) PACl and the mixture of PACl and $PbI_2$. $^{1}$H NMR spectrum of (b) PACl, FAI, and the mixture of PACl and FAI.

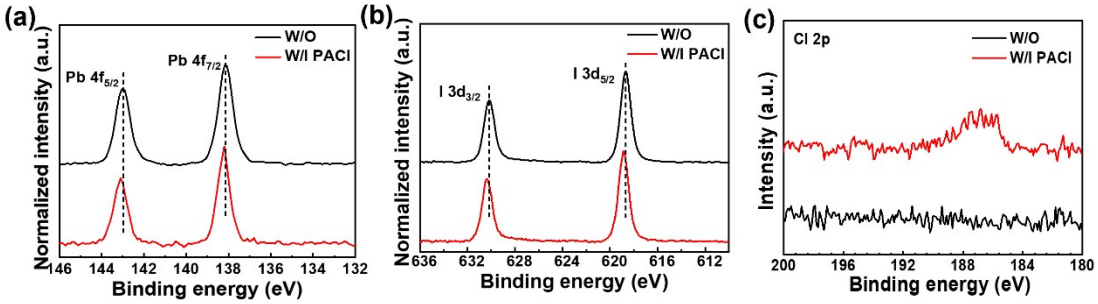


**Fig. S8** (a) Pb 4f, (b) I 3d, and (c) Cl 2p XPS spectra of the perovskite films with and without PACl.

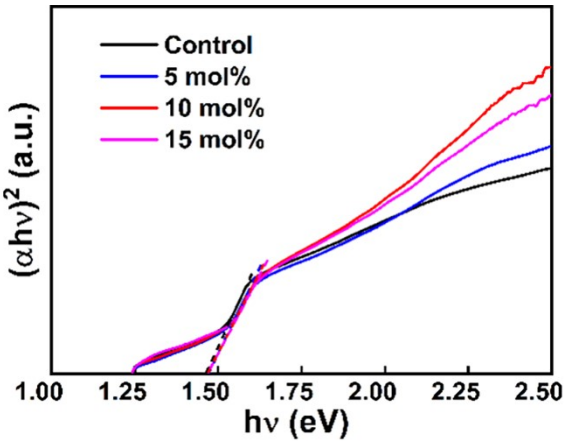


**Fig. S9** Tauc plots of $Cs_{0.1}FA_{0.9}PbI_3$ films without and with PACl.

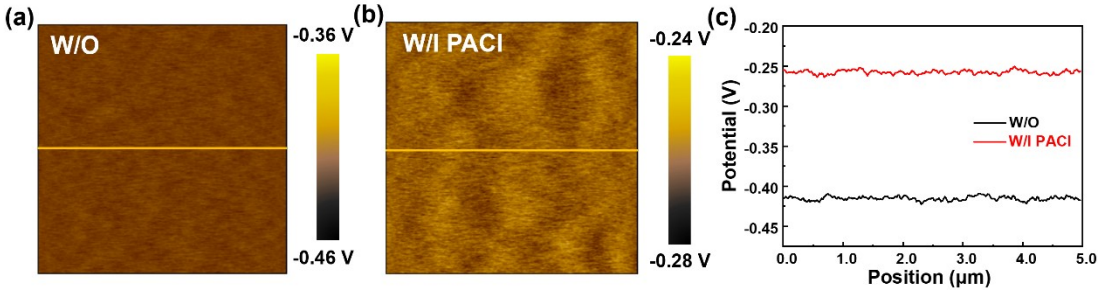


**Fig. S10** KPFM plots of the (a) control and (b) perovskite film with PACl. (c) surface potential along the solid line plotted in (a) and (b).

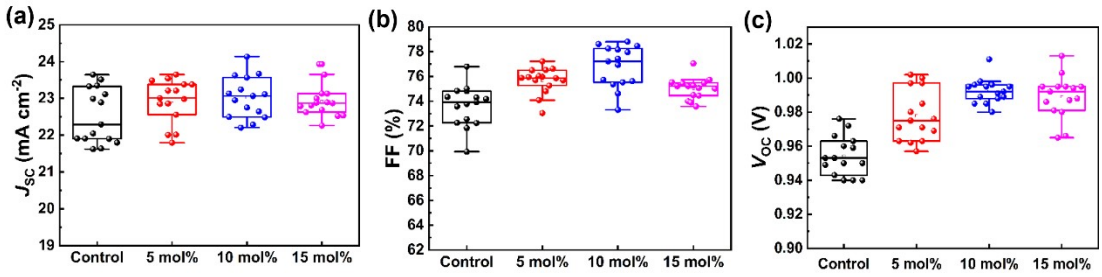


**Fig. S11** Box diagram of (a) $J_{SC}$, (b) FF, (c) $V_{OC}$ under different ratio of PACl.

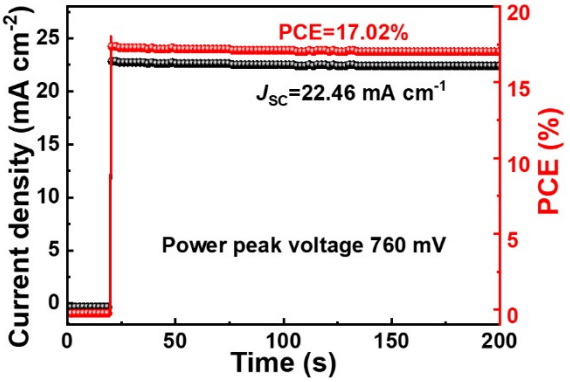


**Fig. S12** Stabilized current density output of PACl-treated $Cs_{0.1}FA_{0.9}PbI_3$ device at a bias voltage of 760 mV.

**Table S1** Statistical photovoltaic performance obtained from 15 cells with different percentages of PACl.

| | | $V_{OC}$ V | $J_{SC}$ mA cm$^{-2}$ | FF % | PCE % |
|---|---|---|---|---|---|
| Control | Avg. | 0.954 ± 0.022 | 22.53 ± 1.12 | 73.63 ± 3.69 | 15.82 ± 0.72 |
| | Max. | 0.940 | 23.51 | 73.77 | 16.31 |
| 5 mol% | Avg. | 0.983 ± 0.019 | 22.89 ± 1.54 | 75.47 ± 3.66 | 16.90 ± 0.52 |
| | Max. | 0.980 | 23.38 | 76.06 | 17.42 |
| 10 mol% | Avg. | 0.992 ± 0.019 | 23.02 ± 1.12 | 76.87 ± 3.57 | 17.55 ± 0.51 |
| | Max. | 0.991 | 24.13 | 75.52 | 18.06 |
| 15 mol% | Avg. | 0.989 ± 0.023 | 22.91 ± 0.65 | 75.03 ± 2.02 | 17.01 ± 0.51 |
| | Max. | 0.988 | 23.65 | 75.53 | 17.64 |

**Table S2** The fitted TRPL parameters of perovskite deposited on the structure of Glass/FTO/m-$ZrO_2$.

| | $\tau_1$ (ns) | $\tau_2$ (ns) | $A_1$ (%) | $A_2$ (%) | $\tau_{avg}$ (ns) |
|---|---|---|---|---|---|
| Control | 0.81 | 6.43 | 16.83 | 83.17 | 5.49 |
| 10 mol% | 1.09 | 8.50 | 11.96 | 88.04 | 7.60 |

**Table S3.** Fitting parameters of the EIS test for the device without/with 10 mol% PACl.

| | $R_s$ (Ω cm$^2$) | $R_{ct}$ (Ω cm$^2$) | CPE1 (F) | $R_{rec}$ (Ω cm$^2$) | CPE2 (F) |
|---|---|---|---|---|---|
| Control | 7.03 | 1014.50 | 7.72 x $10^{-8}$ | 9.50 x$10^4$ | 4.17 x $10^{-6}$ |
| 10 mol% | 6.75 | 771.10 | 2.78 x $10^{-8}$ | 1.95 x$10^5$ | 1.64 x $10^{-6}$ |

**Table S4** Previously reported on the performance of CsFA-based mesoscopic perovskite solar cells with hole-conductor-free.

| No. | Perovskite | $V_{OC}$ (v) | $J_{SC}$ (mA cm$^{-2}$) | FF (%) | PCE (%) | References |
|---|---|---|---|---|---|---|
| 1 | $Cs_{0.2}FA_{0.8}PbI_{2.64}Br_{0.36}$ | 1.07 | 22.6 | 68.3 | 14.3 | [1] |
| 2 | $Cs_{0.1}FA_{0.9}PbI_3$ | 0.92 | 23.63 | 69 | 15 | [2] |
| 3 | $Cs_{0.12}FA_{0.88}PbI_3$ | 0.98 | 23.7 | 75.2 | 17.46 | [3] |
| 4 | $Cs_{0.1}FA_{0.9}PbI_3$ | 0.956 | 24.26 | 76.2 | 17.68 | [4] |
| 5 | $Cs_{0.05}FA_{0.95}PbI_{2.85}Br_{0.15}$ | 0.986 | 23.74 | 78 | 18.33 | [5] |
| **6** | **$Cs_{0.1}FA_{0.9}PbI_3$** | **0.991** | **24.13** | **75.52** | **18.06** | **This work** |

## References


1 Z. F. Wu, Z. H. Liu, Z. H. Hu, Z. Hawash, L. B. Qiu, Y. Jiang, L. K. Ono and Y. B. Qi, *Adv. Mater.*, 2019, **31**, 1804284.

2 X. M. Hou, M. Xu, C. H. Tong, W. X. Ji, Z. Y. Fu, Z. N. Wan, F. Hao, Y. Ming, S. Liu, Y. ~~Hua~~Hu, H. W. Han, Y. G. Rong and Y. Yao, *J. Power Sources*, 2019, **415**, 105–111.

3 J. H. Zhao, H. Z. Wang, L. F. Duan, T. P. Lv, B. Xiao, J. Zhang, J. Liu, Y. M. Zhang and Q. J. Liu, *Sol. RRL*, 2022, **6**, 2100923.

4 J. K. Du, C. Qiu, S. Li, W. H. Zhang, W. H. Zhang, Y. F. Wang, Z. X. Qiu, Q. F. Wang, K. Yang, A. Y. Mei, Y. G. Rong, Y. Hu and H. W. Han, *Adv. Energy Mater.*, 2021, **12**(1), 2102229.

5 Z. W. Zheng, M. H. Xia, X. Y. Chen, X. Xiao, J. W. Gong, J. L. Liu, J. K. Du, Y. R. Tao, Y. Hu, A. Y. Mei, X. H. Lu and H. W. Han, *Adv. Energy Mater.*, 2023, **13**(23) 2204335.